**NUSANTARA BIOSCIENCE**
Vol. 8, No. 2, pp. 232-244
November 2016

ISSN: 2087-3948
E-ISSN: 2087-3956
DOI: 10.13057/nusbiosci/n080216

# *In silico* and *in vivo* wound healing studies of ursolic acid isolated from *Clematis gouriana* against GSK-3 beta

**H. RAJA NAIKA[1,♥], S. BHAVANA[2], JAIME A. TEIXEIRA DA SILVA[3], K. LINGARAJU[1], VIVEK CHANDRA MOHAN[4], V. KRISHNA[5]**

[1]Department of Biotechnology, Tumkur University, Tumkur-572103, Karnataka, India. ♥email: rajanaik1100@gmail.com
[2]Department of Studies and Research in Biochemistry, Tumkur University, Tumkur-572103, Karnataka, India
[3]P. O. Box 7, Miki-cho post office, Ikenobe 3011-2, Kagawa-ken, 761-0799, Japan
[4]Department of Biotechnology, Sri Siddaganga Institute of Technology, Tumkur-572103, Karnataka, India
[5]Department of P.G. Studies and Research in Biotechnology and Bioinformatics, School of Biological Sciences, Kuvempu University, Shankaraghatta-577451, Karnataka, India

Manuscript received: 17 May 2016. Revision accepted: 18 October 2016.

**Abstract.** *Naika HR, Bhavana S, Teixeira da Silva JA, Lingaraju K, Mohan VC, Krishna V. 2016. In silico and in vivo wound healing studies of ursolic acid isolated from* Clematis gouriana *against GSK-3 beta. Nusantara Bioscience 8: 232-244. Clematis gouriana* Roxb. (Ranunculaceae) is an endemic medicinal plant of Western Ghats. Ursolic acid (UA) was isolated from the methanolic extract (ME), which was characterized by spectral studies, and was subjected to *in silico* studies on Glycogen synthase kinase 3-β (GSK3-β) protein, to inhibit protein function. UA showed least binding energy (-13.457 ΔG) towards the binding site and molecular dynamics studies showed minimum potential energy and greater stability with target protein. Thus, UA may be considered as a potential inhibitor of the GSK3-β protein. The wound-healing activity was assessed by excision, incision, and dead space wound models on Wistar strain rats. The results of excision, incision, and dead space wound models showed significant activity. There was a significant increase in skin-breaking strength in rats treated with UA (562.36 ± 7.60 g). The effects of ME and UA on the dead space wound model were pronounced, with a significant increase in the weight of granulation tissue (26.33 ± 0.25 mg), tensile strength (647.00 ± 0.71 g), and hydroxyproline content (1793.83 ± 0.64 µg/100 g). Thus, UA-treated animals showed excellent wound-healing activity. Animals treated with nitrofurazone, ME and UA showed increased collagenation and decreased accumulation of macrophages at the site of injury.

**Keywords:** *Clematis gouriana*, hydroxyproline, molecular docking, molecular dynamics

## INTRODUCTION

Plants contain numerous secondary metabolites that are helpful for humans to treat various ailments. The presence of phytochemicals obtained by screening natural sources such as plant extracts and microbial fermentation has led to the discovery of many clinically useful drugs that play a major role in the treatment of diseases. Natural products obtained from plants have an effective role in the activities of drugs in the interaction between microbes. Plants play an important role in the treatment of some diseases through their antibacterial, antipyretic, hepatoprotective, anticancer, anticoagulant, anti-inflammatory, antiparasitic, wound-healing and immunosuppressant bioactivities (Newman et al. 2003).

Plant-derived material can have an effective and positive role in the treatment of damaged cells during wounding healing (Reinke et al. 2012). In Indian traditional systems of medicine, plants have been used by traditional practitioners to promote wound healing. Many reports on the wound-healing effect of various plant extracts exist, including of *Saussurea lappa* (Ganachari et al. 2005), *Plagiochasma appendiculatum* (Meenakshi et al. 2006), *Terminalia arjuna* (Minakshi and Sushma 2006), *Embelia ribes* (Kumara Swamy et al. 2007), *Lycopodium serratum* (Manjunatha et al. 2007), *Morinda citrifolia* (Vijaykumar et al. 2008), *Calendula officinalis* (Preethi et al. 2009), *Acorus calamus* (Jain et al. 2010), *Ficus benghalensis* (Garg et al. 2011), *Sphaeranthus amaranthoides* (Geethalakshmi et al. 2013), *Citrus hystrix* and *C. maxima* (Abirami et al. 2015), and *Aquilaria agallocha* (Alam et al. 2016). The Wnt/b-catenin pathway can enhance wound healing (Zhang et al. 2008) by inhibiting the Glycogen synthase kinase 3-β (GSK3-β) protein, which is an important regulatory enzyme. To speed up drug research and to improve success rates, research costs should be decreased. Computer-aided drug design (CADD) has become an important means of designing new drugs (Borhani et al. 2012).

In this study, we investigated the wound-healing potential of *Clematis gouriana* Roxb. (Ranunculaceae), a rare woody climber found in the moist deciduous forests of Western Ghats, Karnataka, India. An ethnomedicinal survey in this region revealed that *C. gouriana* is being used by traditional practitioners to cure liver disorders, to heal wounds and inflammation, and as an antipyretic medicine. In the Indian medicine system, or 'Ayurveda', roots of this plant are used to alleviate malarial fever and headaches (Harsha et al. 2013). The roots and stem paste of *C. gouriana* is applied externally for treating psoriasis, itches and skin allergy and the traditional medicine practitioners residing in the vicinity of the Bhadra Wild Life Sanctuary, India, use the leaf and stem juices for treating infectious old wounds, psoriasis, dermatitis, blood

diseases, leprosy, liver disorders, and for healing wounds and cardiac disorders (Manjunatha et al. 2001). This study provides experimental evidence for the ethnomedicinally-based wound-healing properties of this plant. In the present work, we prepared the crude extract of *C. gouriana.* Phytoconstituents, including ursolic acid (UA), were isolated from the methanolic extract (ME) of *C. gouriana*. The ME and *C. gouriana* and isolated compound UA were screened for their wound-healing activity by excision, incision, and dead space wound models. The interaction of UA on GSK3-β was studied using molecular docking and dynamic studies.

## MATERIALS AND METHODS

### Plant material

Leaves of *C. gouriana* were collected from the Lakkavalli reserve forest range of the Western Ghats region of Karnataka, India and identified by Prof. V. Krishna, Kuvempu University. A voucher specimen (KUDB/Ang/ 278) was deposited at the Herbarium of the Department of Applied Botany, Kuvempu University, India.

### Extraction and isolation

The shade-dried powdered leaves were subjected to successive solvent extraction as described next. Powdered dry leaves were placed in a one-liter Soxhlet apparatus and extracted successively with methanol (50-80°C; Merck Mumbai, India) for 72 h in four batches of 250 g each. The extracts were filtered and concentrated in vacuum using a rotary flash evaporator (Büchi, Flawil, Switzerland). Leftover solvent was completely removed in a water bath and finally dried in a desiccator. The crude extracts obtained from each of the solvents were stored in an airtight container until further use.

The chemical constituents of ME were evaluated by qualitative tests (Trease et al. 1983). A pinch of crude extract was completely dissolved in methanol and the extract was subjected to solvent standardization by thin layer chromatography (TLC) using different solvents such as methanol and chloroform in the ratio of 8.5:1.5. After the clear separation of different bands on TLC plates (Harsha Enterprise, Mumbai, India), the same solvent system was used for column chromatography. The mobile phase consisted of methanol: chloroform (8.5:1.5) to separate the compound. The purity of the isolated UA was almost 67%.

### Characterization

The melting point of the isolated UA was determined by using a melting point apparatus (Jindal, New Delhi, India). UV spectroscopy of the compounds was performed with a 1700UV spectrophotometer (Shimadzu, Kyoto, Japan). IR spectra were recorded with KBr pellets on a Perkin-Elmer 1710 FT-IR spectrophotometer. $^{1}$HNMR spectra of the compound were obtained on a Bresker AMX (400 MHz) NMR spectrometer using $CDCl_3$ and methanol as solvents and mass spectra were recorded on a MAT 312 spectrophotometer and FAB-MS (positive) data on a JEOL SX 102/DA-600 at the Central Drug Research Institute (CDRI), Lucknow, India. The structure of the compound was characterized based on all spectral data.

### *In silico* studies

The crystal structure of glycogen synthase kinase 3-β (PDB ID: 1Q5K) was retrieved from the protein data bank (Weiss et al. 2013). Protein optimization studies were carried out using steepest descents and conjugate gradients method for 2000 cycles, RMS gradient 0.1, energy changes 0.0 and the lowest energy model was selected for further analysis and validation (Kepp et al. 2014). The ligands were designed and the structures were analyzed using a Marvin sketch (Mahanta et al. 2013). Minimization of ligands (UA and a standard compound, nitrofurazone) was carried out using CHARMm and MMF force field using the minimization protocol in DS 3.5 (Guo et al. 2013). Drug-likeness was evaluated using the Lipinski rule of five (Amin et al. 2013). Absorption, distribution, metabolism, and excretion (ADME) was carried out using the ADME (Arafat et al. 2014) pipeline in DS3.5. Toxicity prediction was carried out using TOPKAT (Pizzo et al. 2013). All activities were performed using Discovery Studio 3.5 (Patronov et al. 2011). The molecular docking studies were carried out to investigate the binding affinities and interaction modes between ligands and target using Lead IT (FlexX) (Chowdhury et al. 2013). The target proteins were uploaded to the Lead IT protein preparation workspace. The active site amino acids were defined in the target molecule during the target preparation step of FlexX. A sphere of 10Å radius was defined as the active site. UA and nitrofurazone were loaded in Lead IT as the docking library. The docked ligand-target complexes were analyzed to identify the interactions and binding affinities. The docking score was recorded and docking poses were saved for reference. The docked structure was visualized using Discovery Studio 3.5. The docked ligand-target complexes were analyzed carefully to identify the interactions and binding affinities. The docking score was recorded and docking poses were saved for reference. Sample preparation was conducted under the following parameters: [minimization] steepest descent and conjugate gradient: each with maximum steps of 500, [heating time] 50 ps, [equilibration time] 200 ps. The simulations were produced with a total production time of 20 ns with NVT, a temperature decay time of 0.4 ps, and a target temperature of 310 K. Root mean square deviations (RMSD) of the protein-ligand complex, potential energy of the protein-ligand complex and the H-bond distance were analyzed using the Analyze Trajectory function following MD simulation (Amjad-Iranagh et al. 2014).

### Drug formulations for wound healing activity

Two types of drug formulations were prepared from ME and UA. For topical administration, 200 mg of the crude, dark-green ME was mixed with 100 g of sodium alginate to obtain a 0.2% (w/w) gel. Similarly, 100 mg of UA was incorporated with 50 g of sodium alginate to obtain a 0.2% gel. For oral administration, suspensions of 30 mg/mL of ME and 4 mg/mL of UA were incorporated with 1% (w/v) gum tragacanth (SD Fine Chemicals, Bangalore, India).

**Selection of rats**

Wistar rats of either sex, weighing between 50-200 g, were procured from the central animal house, National College of Pharmacy, Shimoga, Karnataka, and were used for all studies. The rats, housed at six per polypropylene cage, were fed with a commercial diet (Hindustan Lever Ltd., Bangalore, India) and water was provided *ad libitum* throughout the experiment except for a short fasting period before the study started. The study was approved by the Institutional Ethical Committee on 15th November 2007 (Registration Number 144/1999/CPCSEA/SMG). The staircase method (Ghosh et al. 1984) was adopted to determine acute toxicity. Healthy Wistar rats of either sex weighing 20-25 g were used to determine the safest dose. Gum tragacanth (1%, w/v) was used as the vehicle to suspend ME, and UA and feeding were performed orally using a 7.62 cm stainless steel feeding needle (Harvard Apparatus, Holliston, MA, USA).

**Wound-healing activity**

Six Wistar rats of either sex were used for each experimental group (I, control; II, standard; III, ME; IV, UA). This grouping was used for the excision, incision and dead space wound models. The rats of group I were considered as the control while those of group II served as a reference standard and were treated with 0.2% (w/w) nitrofurazone ointment (Eskeyef, Mumbai, India). The rats of group III were treated with *C. gouriana* ME while those of group IV were treated with UA.

**Excision wound model**

The excision wound model, which is employed to assess the potency of a drug to promote wound healing in 'trauma' types of wounds, was assessed by: (i) the rate of wound contraction; (ii) the number of days required for complete epithelialization of the wound area. Rats were inflicted with excision wounds as described by Morton et al. (1972) under light ether anesthesia. In this model, the skin of the impressed area was excised to full thickness on the dorsal thoracic region of the rats to obtain a wound area of about 500 $mm^2$. The ointment gel was topically applied daily until complete epithelialization started from the day of operation. Wounds were traced on graph paper graded in $mm^2$ on days 4, 8, 12 and 16 and thereafter on alternate days until healing was complete. Wound closure was measured every four days at regular intervals up to 16 days to assess the percentage of wound closure and time to achieve epithelialization. These parameters indicate the formation of new epithelial tissue that covers the wound. The percentage of wound closure was calculated using the formula: % wound reduction = [Wound area day 0 - Wound area on respective day] / [Wound area day 0] × 100. The number of days required for senescence of the scar without any residual of the raw wound indicated the period of epithelialization.

**Incision wound model**

In the incision wound model (Ehrlich et al. 1969), 6-cm long paravertebral incisions were made through the full thickness of the skin on either side of the vertebral column of the rat, ensuring that the incision was at least 1 cm lateral to the vertebral column. The wounds were closed with interrupted sutures 1 cm apart using a surgical thread (No. 000) and curved needle (No. 11) (Ramana Surgical, Bangalore, India). The wounds were left undressed and drugs were topically applied to the wound once a day, until healing was complete. The skin-breaking strength of the 10-day-old wound was measured by the continuous water technique of Lee and Tong (1968) using a tensiometer (Ramana Surgicals, Bangalore, India). Skin-breaking strength was expressed as the minimum weight (in g) of water necessary to bring about gaping of the wound.

**Dead space wound model**

In the dead space wound model, rats were divided into three groups containing six rats each. The rats of group I, which served as the control, were treated orally with 1 mL/kg body weight (bw) of 1% gum tragacanth. The rats of groups II and III were treated with an oral dose of ME (30 mg/kg bw) and UA (4 mg/kg bw), respectively. The rats were lightly anesthetized with ether, and dead-space wounds were created by subcutaneous implantation of sterilized cylindrical grass or wood piths (2.5 cm×0.3 cm), one on either side on the dorsal paravertebral surface of the rats (Patil et al. 2004). The granulation tissues that formed on the grass or wood piths were removed on the 10th post-wounding day (PWD). These tissues were subjected to breaking strength and histological studies. Hydroxyproline (HYP) (Hi Media, Mumbai, India) content was estimated calorimetrically to evaluate the effect of ME and UA on collagen formation. Neutral formalin solution (10%, v/v) was used to fix granulation tissues for 24 h and dehydrated with an ethanol-xylene series (Kanai et al. 2000). The dehydrated granulation tissues were embedded in paraffin at 40-60°C. Sections 10 µm in thicknesses were made with an ultramicrotome (Thermo Scientific, Bangalore, India). The sections were stained with hematoxylin-eosin and observed under a microscope (SXZ10, Olympus, India).

**Data analyses**

Data from these experiments (i.e., all three models) are expressed as the mean ± standard error of six animals in each group. The data were evaluated by one-way analysis of variance (ANOVA) followed by Tukey's pair-wise comparison test by using SPSS statistical software version 11 (SPSS Inc. Chicago, USA).

**Estimation of hydroxyproline content in granulation tissue of rats**

HYP content was estimated from the granulation tissue of rats from the dead space wound model after its harvest from the pith according to (Woessner et al. 1963). Initially, a standard curve was prepared, as explained next. Six test tubes were prepared, each containing 2.0 mL of distilled water (blank) and 3, 4, 6, 8 and 10 µg of HYP from a stock solution of 100 µg/mL. To this solution, 2 drops of methyl red (Hi Media) were added to each of the test tubes and mixed properly and a theoretical amount of 2.5N sodium hydroxide (Hi Media) was added. Titration was carried out with dilute hydrochloric acid and sodium hydroxide such

that the color in the test tubes changed from pink to yellow corresponding to pH values of 6-7. One mL of chloramine-T solution (Hi Media) was sequentially added to each tube. The contents were mixed and allowed to stand for 20 min at room temperature. One mL of perchloric acid (Hi Media) was added to each test tube in the same order. The contents were mixed and allowed to stand for 5 min. One mL of *p*-dimethylamino benzaldehyde (Hi Media) solution was added to each test tube and shaken until no color could be seen. All test tubes were placed in a 60°C water bath for 20 min then cooled under tap water for 5 min. The absorbance of the solution was determined colorimetrically (Shimadzu-1700, Kyoto, Japan) at 570 nm to obtain a standard curve.

Granulation tissue (300 mg) was homogenized in a glass homogenizer with 10 mL of 6N hydrochloric acid and transferred to 25-mL glass ampoules. The ampoules were sealed and hydrolyzed for 3 h at 130°C. The contents were decanted to graduated glass cylinders. The ampoules were washed thoroughly with water and the contents were combined with the hydrolysate. Then they were processed in a similar manner as samples of the standard curve. After titration, the samples were diluted with distilled water to 50 mL such that 2 mL of these samples contained 1-10 µg of HYP, assessed as indicated above. The HYP content of the granulation tissue of the ME and UA was calculated from the standard curve.

## RESULTS AND DISCUSSION

The yield of the ME in *C. gouriana* leaves was 0.08% (64 g/800 g powder). The crude extract was qualitatively analyzed, testing positive for glycosides, terpenoids, and proteins. The extract was subjected to TLC to separate bands and to standardize the solvent system. Methanol and chloroform in an 8.5:1.5 ratio showed a very clear and dense band in TLC. The extract was subjected to column chromatography using the same solvents in the same ratio, yielding a brown crystalline compound which was labeled as CGME (*Clematis gouriana* methanol extract). The yield of the compound was 22.5% (450 mg/20 g of crude extract of *in vivo* leaves). The compound showed positive results for Salkowaski and Liebermann-Burchard tests and was found to be a triterpenoid with a melting point of 289°C. The compound was characterized using the following spectral studies.

### Spectral characteristics

IR (KBr) revealed the following: 3434.8 $cm^{-1}$ (br, OH), 2926.0 $cm^{-1}$, 2368.5 $cm^{-1}$ (C-H str. in $CH_3$ and $CH_2$), 1749.7 $cm^{-1}$ (C=O str. of COOH group), 1595.2 $cm^{-1}$ (C=C str.), 1350.1 $cm^{-1}$ (C-H deformation in gem dimethyl), 1059.3 $cm^{-1}$ (C-O str. of secondary alcohol) (Figure S1). $^1$HNMR ($CDCl_3$) revealed the following: δ 0.88 to δ 0.9 (m, methyl protons), δ 1.29 to δ 1.93 (m, 25H for $CH_2$ and CH protons), δ-1.3, 2H (cyclohexane), δ-2.0, 1H (O-H of alcohol), δ-4.52 (olefinic protons), δ-11.0 (1H (O-H of COOH) (Figure S2).

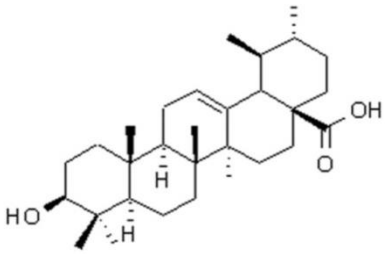


**Figure 1.** Structure of ursolic acid

### Mass spectra ($ES^+$)

The mass spectrum showed a molecular ion peak at m/z 475 (4%). Other peaks appeared at 424 (14.58%), 423 (56.25%), 407 (46.87%), 385 (7.29%), 331 (6.25%), 317 (9.15%), 219 (10.13%), 182 (8.74%), 181 (43.75%), 168 (18.75%), 149 (20.62%), 130 (54.16%), 100 (22.91%), 91 (55.20%), 84 (100%) and 41 (41.6%) (Figure S3). The IR spectrum of the compound Code-CGM showed absorption bands at 3434.8 $cm^{-1}$ for the hydroxyl group and 2926.0 and 2368.5 $cm^{-1}$ for the terminal methylene groups. The $^1$H NMR spectrum revealed the presence of terminal methyl groups at δ 0.88 to 0.9 and a multiplet at δ 4.52 due to olefinic protons. The $ES^+$ mass spectrum showed a molecular ion peak at m/z 457 correspondings to the molecular formula $C_{30}H_{48}O_3$. From the above spectral data, compound Code-CGME was identified as UA (Figure 1).

### *In silico* activity

The crystal structure of GSK3-β, which was obtained from the protein data bank (1Q5K), had three domains, a crystallographic resolution of 2.00 Å, and a molecular weight of 17153.2 Da. The initial and final potential energy, which was calculated by energy minimization, was found to be 108010.13 and -21233.81 kcal/mol, respectively. The crystal structure of GSK3-β includes an active site region depicted in Figure 2A. The green color mesh surface is the binding area and the violet color indicates active site residues (Figure 2B).

UA extracted from *C. gouriana* was selected as a candidate based on its high docking score compared to nitrofurazone, the standard compound. The 3D images of selected and standard compounds (UA and nitrofurazone, respectively) are shown in Figure 3. UA should be more easily absorbed by the human body than nitrofurazone as indicated by adsorption and blood-brain barrier properties. UA satisfied ADME and TOPKAT studies, these results demonstrating its potential as a drug-like molecule. The Discovery Studio 3.5 small molecular pipeline was used to analyze drug-likeness (ADME and TOPKAT) (Table 1.A, 1.B). UA and nitrofurazone were subjected to FlexX molecular docking studies and molecular docking scores are listed in Table 2. UA had good affinity to the active site residue of 1Q5K. The binding mode of UA with the X-ray crystal structure of 1Q5K is presented (Figure 4). UA interacted with target protein (LEU187 and GLU185) with the least energy (-13.457 ΔG) while the standard compound nitrofurazone interacted with target proteins (ASP133 and TYR134) with an energy value of -3.897 ΔG.

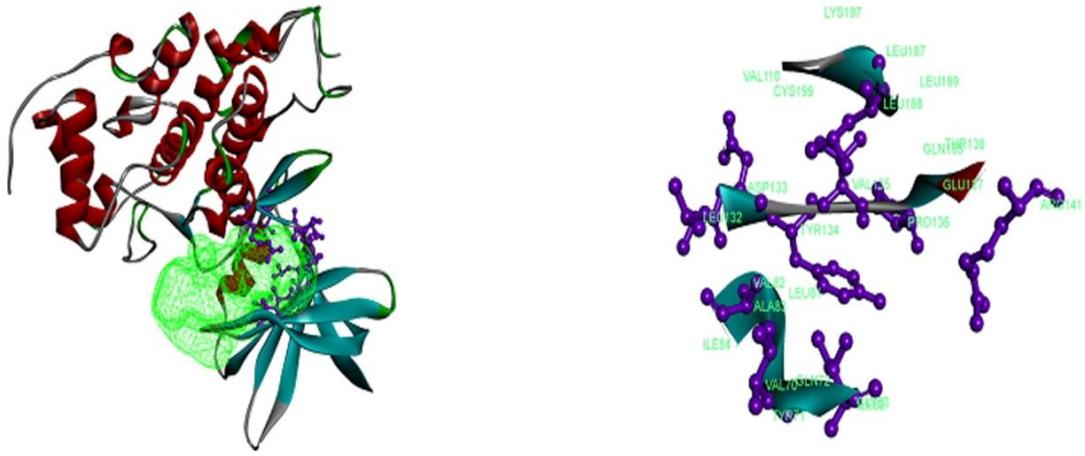


**Figure 2.** X-Ray crystal structure of selected target protein. (A) Crystal structure of Glycogen synthase kinase 3-β complexed with inhibitor (1Q5K). (B) Active site of target protein (violet color - active site residue)

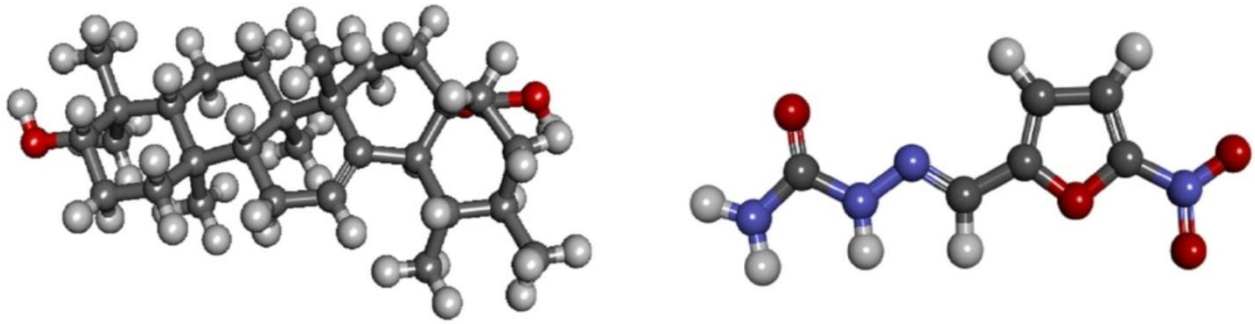


**Figure 3.** 3D structure of ursolic acid and nitrofurazone compound. A. Ursolic acid, B. Nitrofurazone

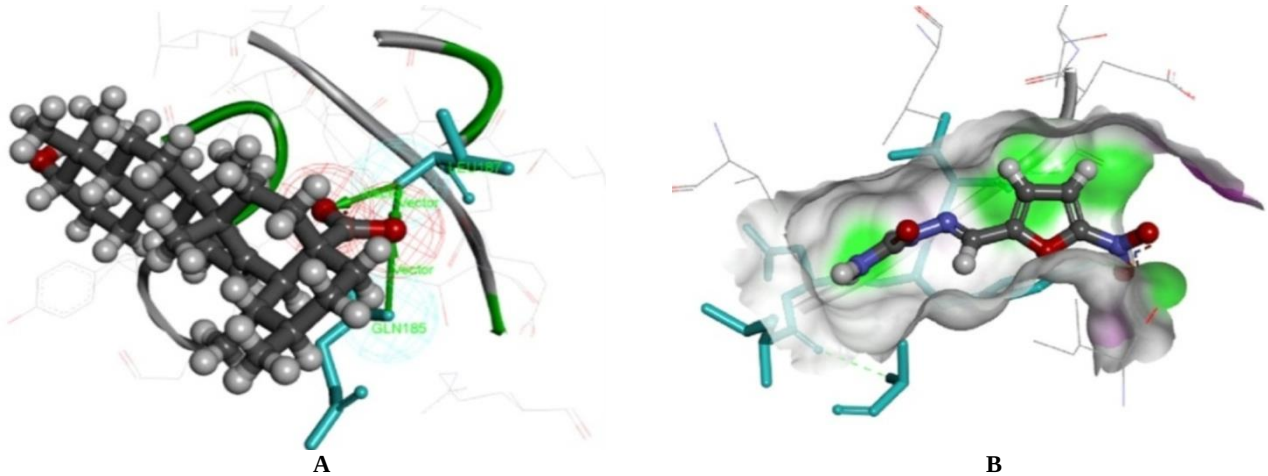


**Figure 4.** Binding mode of ursolic acid (-13.457) with X-ray crystal structure of 1Q5K (-8.781). A. Ursolic acid interacted with protein. B. Standard compound interacted with protein.

**Table 1.A.** ADMET results of selected compound and standard compound

| Compound name | ADMET solubility level | ADMET BBB level | ADMET EXT CYP2D6 | ADMET EXT hepatotoxic | ADMET absorption level | ADMET EXT PPB | ADMET AlogP98 | ADMET PSA 2D |
|---|---|---|---|---|---|---|---|---|
| Ursolic acid | 1 | 4 | -4.36461 | -10.0226 | 1 | 1.6932 | 6.492 | 58.931 |
| Nitrofurazone | 4 | 4 | -9.93387 | 1.49793 | 3 | -14.9479 | 0.223 | 123.351 |

**Table 1.B.** TOPKAT results of selected compound and standard compound

| Compound name | NTP Carcinogenicity call (male mouse) (v3.2) | NTP Carcinogenicity call (female mouse) (v3.2) | Developmental toxicity potential (DTP) (v3.1) | Skin irritation (v6.1) | Ames mutagenicity (v3.1) |
|---|---|---|---|---|---|
| Ursolic acid | 0.000 | 0.000 | 0.000 | 0.000 | 0.000 |
| Nitrofurazone | 0.000 | 0.099 | 0.000 | 0.360 | 0.000 |

**Table 2.** Results of protein-ligand docking score using the FlexX tool

| Protein | Compound name | Lead IT score |
|---|---|---|
| 1Q5K | Ursolic acid | -13.457 |
| | Nitrofurazone | -8.781 |

Molecular simulations were performed on the crystal structure of the docked complex structure. The molecular dynamics conformation of UA and nitrofurazone at 0 and 6 ns helped to visualize the interactions involved in protein-ligand complex stability. After the molecular dynamics run, UA and nitrofurazone remained closely bound to the GSK3-β domain. Each frame collected from the trajectory file was aligned to the first one based on their backbone atoms. The distributions of potential energy and C-alpha RMSD values are presented in Figure 5A and 5B. Figure 5A represents the potential energy of UA and nitrofurazone. UA was most stable by maintaining potential energy of around -830 to -900 kcal mol and maintaining a ligand RMSD of approximately 1 Å compared to nitrofurazone, which had an RMSD of 2 Å. The interaction of UA on GSK3-β was studied using molecular docking and dynamic studies. *In silico* studies showed that UA is a potential inhibitor for wound healing.

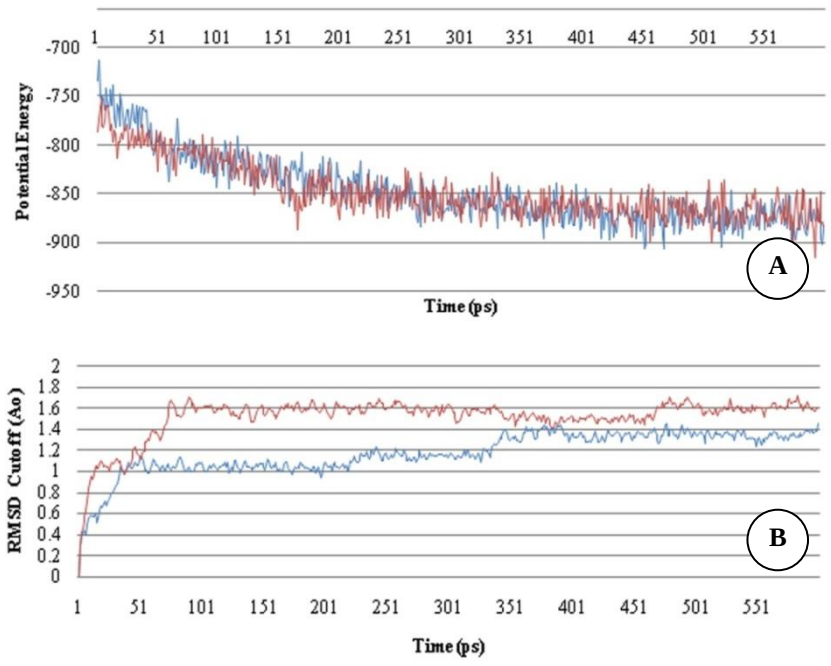


**Figure 5.** A. Potential energy of docked complex. B. RMSD of docked complex. Blue = ursolic acid; red = nitrofurazone standard

**Table 3.** Effect of methanolic extract (ME) and ursolic acid (UA) of *Clematis gouriana* on percentage closure of excision wound area ($mm^2$ ± SE)

| Group | 4th day | 8th day | 12th day | 16th day | Mean time of epithelialization (days) |
|---|---|---|---|---|---|
| | | | (%) | | |
| Control | 25.05 ± 0.56 | 54.23 ± 3.14 | 73.03 ± 3.00 | 83.50 ± 1.08 | 24.12 ± 0.28 |
| Nitrofurazone | 43.44 ± 1.73 b | 76.40 ± 0.24 b | 86.12 ± 0.15 a | 98.86 ± 0.24 b | 17.54 ± 0.10 b |
| ME | 37.02 ± 0.68 b | 75.30 ± 1.13 b | 88.21 ± 3.11 b | 94.42 ± 1.36 b | 18.28 ± 1.17 b |
| UA | 23.65 ± 0.96 b | 73.40 ± 1.05 b | 83.72 ± 1.35 b | 94.25 ± 1.52 b | 19.52 ± 1.05 a |
| *F*-value | 20.09 | 13.65 | 6.55 | 29.46 | 12.16 |

Note: Each value represents mean ± SE of 6 animals. Significance: a, $P<0.05$ or b, $P<0.01$ when compared to the control

**Wound-healing activity**

Wound-healing involves four phases: granulation, wound contraction, collagenation and scar formation (Azad 2002). Three different models (excision, incision and dead space wound) were used in our study to assess the effect of ME and UA at different stages of wound healing which ran concurrently, but independent of each other. In all three models, significantly improved wound-healing activity was observed with ME and UA more than with nitrofurazone and the control group of rats. There was almost complete healing on the 18th PWD with ME and UA. The period of epithelialization and percentage of wound contraction due to the effect of *C. gouriana* ME is shown in Table 3.

The animals treated with *C. gouriana* ME showed a significant reduction in wound area (94.42%) and faster rate of epithelialization (18.28 ± 1.17 days). In control animals, the duration of healing was extended to 24 days and on the 16th PWD, epithelialization was complete in animals treated with nitrofurazone, showing 98.86% wound contraction (UA-treated animals showed 94.25% wound contraction and a rate of epithelialization in 19.52 ± 1.05 days, and the control took 24.12 days). Thus, ME and UA significantly reduced the wound area. The scar area of ME was 94.42% and that of UA was 94.25% while the time required for complete epithelialization of the excision wound was 16 days. This confirms that ME and UA were significantly better than the control, which accounted for 83.50% of the scar area by the 16th PDW. Wound contraction was faster and complete epithelialization of the excision wound was observed on the 18th PDW in drug-treated animals while a weaker healing effect on excision wounds was observed in control animals.

In the incision model, an incision wound was made on the paravertebral region of the rat that had been sutured. An important parameter employed in the assessment of the incised wound is the measurement of wound strength which can be measured by the skin-breaking strength of the incised wound on the 10th PWD using a tensiometer. The crude ME extract of *C. gouriana* leaves showed a significant increase in tensile strength on the 10th PWD (574.85 ± 2.08 g) compared to the control (403.00 ± 23.23 g) (Table 4). UA showed a significant increase in skin-breaking strength in the rats treated with it (562.36 ± 7.60 g). The animals treated with nitrofurazone showed a significant increase in tensile strength of the incision wound (656.18 ± 21.95 g).

The effects of ME and UA on the dead space wound model were assessed by an increase in the weight of granulation tissue, increase in its tensile strength and HYP content of the granulation tissue. As in the excision and incision wound models, the ME of *C. gouriana* exhibited highest wound-healing property, revealed by the significant increase in dry weight of the granulation tissue, increased tissue-breaking strength and increased HYP content (Table 5). UA-treated rats demonstrated excellent wound-healing ability, with a significant increase in dry weight of the granulation tissue, increased tissue breaking strength and increased HYP content relative to the control (Table 5).

**Table 4.** Effect of methanolic extract (ME) and ursolic acid (UA) of *Clematis gouriana* on healing of incision wound

| Group (N) | Breaking strength (g) |
|---|---|
| Control | 403.00 ± 23.22 |
| Nitrofurazone | 656.18 ± 21.95 b |
| ME | 574.85 ± 2.08 b |
| Ursolic acid | 562.36 ± 7.60 b |
| *F*-value | 14.34 |

Note: Each value represents mean ± SE of 6 animals. Significance: a, $P<0.05$ or b, $P<0.01$ when compared to the control

**Table 5.** Effect of methanolic extract (ME) and ursolic acid (UA) of *Clematis gouriana* on healing of dead space wound

| Group (N) | Wet weight of granulation tissue (mg) | Dry weight of granulation tissue (mg) | Tissue-breaking strength (g) | Hydroxyproline content (µg/100g) |
|---|---|---|---|---|
| Control | 80.53 ± 2.26 | 12.36 ± 0.43 | 354.12 ± 9.21 | 1358.78 ± 36.09 |
| Nitrofurazone | 134.78 ± 1.89 b | 26.73 ± 0.42 b | 697.37 ± 38.23 b | 2468.10 ± 0.82 b |
| ME | 122.93 ± 0.67 b | 26.33 ± 0.25 b | 647.00 ± 0.71 b | 1793.83 ± 0.64 b |
| Ursolic acid | 88.02 ± 0.72 a | 21.02 ± 0.70 b | 657.12 ± 19.12 b | 1455.93 ± 0.60 b |
| F-value | 207.70 | 130.44 | 56.75 | 113.95 |

Note: Each value represents mean ± SE of 6 animals. Significance: a, $P<0.05$ or b, $P<0.01$ when compared to the control

Histological studies of the granulation tissue of the control group of rats (Figure 6A) indicate the presence of acute inflammatory cells, fibroblastic connective tissue, very few blood vessels, little epithelialization, fibrosis, collagen formation and lower HYP content, indicating incomplete healing of the wound in control rats. The rats treated with nitrofurazone showed significant collagenation and excess accumulation of macrophages at the site of injury (Figure 6B).

The ME of *C. gouriana* showed a significant increase in collagenation and a reduced accumulation of macrophages (Figure 6C). In UA-treated rats the histology of granulation tissue showed complete healing with more fibroblasts, a significant increase in collagen tissue, improved number of blood vessels and a substantial increase in the weight of the granulation tissue, HYP content and breaking strength, similar to nitrofurazone-treated rats (Figure 6D).

Significant wound-healing activity was observed in both groups of rats treated with ME and UA (Table 3). The percentage of wound closure was significant in rats treated with UA (83.72 ± 1.35) on day 12 and 94.25 ± 1.52 on day 16. In control animals, these values were only 73.03 ± 3.00 and 83.50 ± 1.08, respectively. The time required for complete epithelialization of the excision wound is an important parameter to assess the wound-healing process. The mean time taken for complete epithelialization of the excision wound in the UA-treated group was less than in rats treated with ME (Table 3). The promotion of wound healing activity was also clearly observed by the tensile strength of the incision wound, which increased significantly in the animals treated with UA, similar to those treated with nitrofurazone. A moderate gain in tensile strength was observed in ME-treated rats but was insignificant in the control group. The effect of oral administration of UA and ME on the dead space wound model was assessed by the increase in weight of granulation tissue and the upsurge in its tensile strength (Table 5). This indicates enhanced collagen maturation by improved cross-linking of collagen fibers, which were observed in histopathological sections (Figure 6C, 6D). The increased weight of the granulation tissue also indicated higher protein content (Table 5). Among these treated rats, wound-healing activity was highest in UA-treated animals.

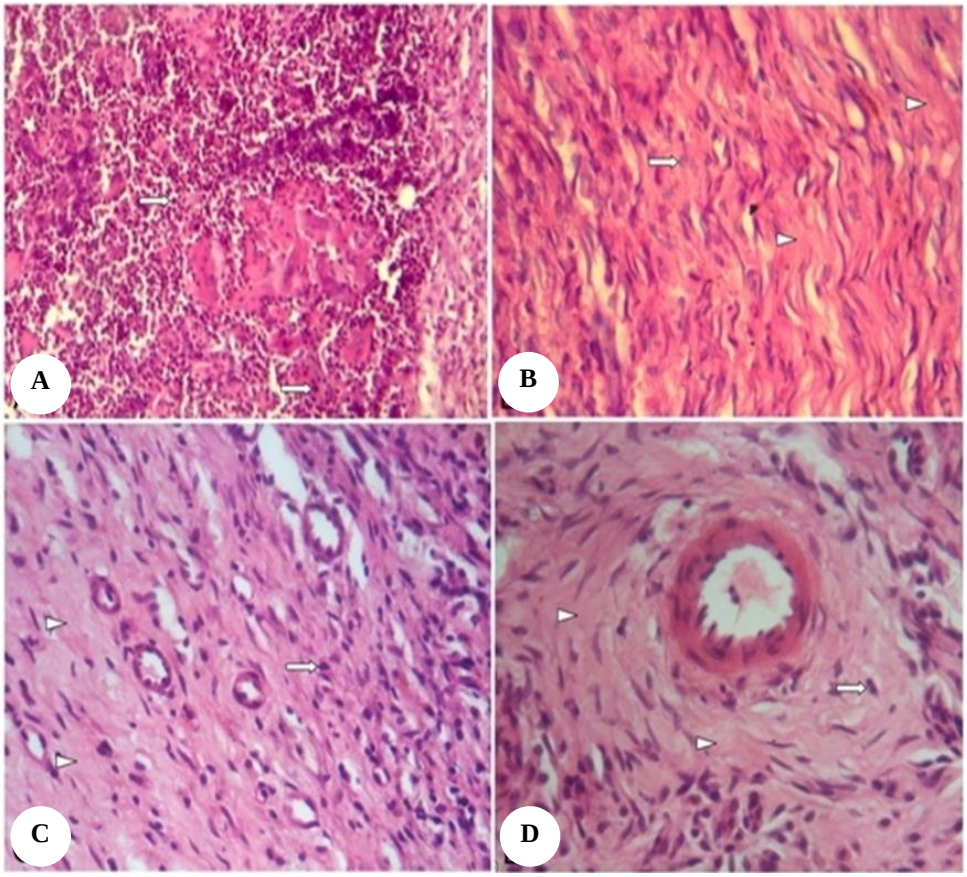


**Figure 6.** A. Histopathological section of wound healing activity using hematoxylin and eosin (H&E) stain (10×). B. Histological section of granulation tissue of standard skin ointment nitrofurazone-applied on rats showing complete epithelialization. Arrowhead indicates the deposition of collagen fibers (H&E, 10×). C. Histological section of the granulation tissue of methanolic extract-treated animal showing moderate epithelialization and collagenation. Arrows indicate the retention of macrophages with moderate epithelialization, fibrosis and arrowhead showing collagen formation (H&E, 10×). D. Histological section of the granulation tissue of ursolic acid-treated animal removed after 10th day of treatment showing complete epithelialization and increased collagen deposition. Arrowhead showing increase in collagen formation and complete healing with more fibroblasts (H&E, 10×).

**Discussion**

In this paper, an *in silico* study, molecular docking and simulation were used to rank a compound, UA, isolated from *C. gouriana* leaves according to its binding energy with GSK3-β protein. Simulation studies were used to analyze the conformation of UA inside the binding site of proteins and to show how these compounds bind. UA was subjected to molecular docking and dynamics studies. Docking and dynamics studies showed that UA significantly inhibited GSK3-β protein, and displayed least binding energy (-13.457 ΔG) with good affinity towards the binding pocket. Molecular dynamic studies indicated that UA had minimum potential energy and was more stable with target protein than the standard compound, nitrofurazone. *In silico* studies thus showed that UA is a potential enhancer of wound healing.

The crude ME extract and UA of *C. gouriana* was concomitantly used to assess wound-healing activity. Wound healing is a complex cellular event by which damaged tissue is restored as closely as possible to its normal state. The healing process depends upon the reparative ability of the tissue, the type and extent of damage and the general state of health of the tissue. Three different models were used in our study to assess the wound-healing effect of ME and UA on various phases of wound healing. In the excision wound model, significant wound-healing activity was observed in the animals treated with ME and UA. A significant decline in the period of epithelialization and increase in wound contraction rate was observed in rats in the excision wound model. In rats treated with UA and nitrofurazone, epithelialization was complete on the 16$^{th}$ PWD. In control rats, in contrast, the rate of wound contraction was slow and complete epithelization of the excision wound was extended up to the 20$^{th}$ PWD. Breaking strength is the strength of a healing wound and is measured experimentally by the amount of force required to disrupt it. Initially, a wound will have little breaking strength because the clot alone will be holding the edges together. Thereafter, breaking strength significantly increases rapidly as collagen deposition increases and cross-linkages are formed between the collagen fibers (Romero-Cerecero et al. 2013). The results of the present study clearly indicated that ME and UA enhanced healing of all three types of cutaneous wounds. Similar work was carried out by many investigators. Singh et al. (2012) evaluated the wound-healing activity of the ethanolic leaf extract and deoxyelephantopin isolated from *Ocimum basilicum*. Both the ethanolic extract and deoxyelephantopin exhibited significant wound healing activity in excision, incision, and dead space wound models. Pather et al. (2011) studied the MEs of *Bulbine natalensis* and *Bulbine frutescens* (Asphodelaceae) on cutaneous wounds. In the excision wound model, wound contraction and the time is taken for complete epithelialization by the extracts and deoxyelephantopin was 92.4% (16.6 days) and 98.8% (14 days), respectively. The skin breaking strength in the incision model was 380 and 412 g, respectively. The dry weight of granulation tissue and its tensile strength increased considerably after oral administration of ME (61.6 mg/100 g and 398 g, respectively) and deoxyelephantopin (74 mg/100 g and 437 g, respectively). They used nitrofurazone ointment as the standard reference drug. Similarly, Manjunatha et al. (2005) reported the wound-healing potency of *Vernonia arborea*. In their study, different leaf extracts were assessed using excision, incision, and dead space wound models. Among the extracts, ME showed excellent wound-healing activity evidenced by 100% closure of the excision wound on 18$^{th}$ PWD. ME exhibited equally significant healing activity when compared with that of the standard drug framycetin sulphate. Nayak et al. (2006) reported the wound-healing activity of *Catharanthus roseus* flower extract. The extract at a dose of 100 mg/kg body weight significantly promoted all excision, incision, and dead space wound models. In the excision wound model, the percentage of wound closure and the period of complete epithelialization were 65.40% and 10.20 days, respectively. In the incision wound model the extract exhibited significant healing activity. The skin breaking strength was 445.0 g. In the dead space wound model the tensile strength of granulation tissue increased to 98.60 g and the dry weight of granulation to 7.4 mg. Kumar et al. (2013) tested the excision, incision, and dead space wound healing activity of embelin isolated from the ethanolic extract of *Embelia ribes* leaves. The percentage of wound closure was significant (89.33%) in animals treated with embelin on day 12 and 98.50% on day 16 while in control animals it was only 68.17% and 85.33%, respectively. The percentage of wound closure on the 16$^{th}$ PWD and the period of complete epithelialization after topical application of the extract and embelin on the excision wound model was 97% (18.67) and 98.5% (18.17), respectively. In the incision wound model, skin-breaking strength for the extract and embelin was 495 and 528 g, respectively. They compared these results with the standard reference drug framycetin. The effect of the ethanolic extract and embelin on tissue tensile strength in the dead space wound model was 501.67 g and 81.00 g, respectively. The dry weight of granulation tissue increased significantly and for the ethanolic extract and embelin it was 70.17 and 81 mg/100 g of tissue, respectively.

Wound healing is the physiological response to tissue injury that results in the replacement of destroyed tissue by living tissue and thus restoration of tissue integrity (Anthony et al. 2007). Rubin et al. (1963) stated that wound healing occurs as follows. Wound contraction initially begins slowly. After 3 or 4 days, rapid wound contraction occurs. Collagenization increases rapidly during the mid-phase. The myofibroblasts present in the margins of the wounds appear to constitute the machinery for wound contraction. These are responsible for moving the overlying debris. Epithelialization of the wound mainly occurs by proliferation and migration of the marginal basal cells lying close to the wound margin. The hematoma within the wound is soon replaced by granulation tissue, which consists of new capillaries and fibroblasts. The freshly formed capillary loops release protein and thus the tissue fluid which is formed is a very suitable medium for fibroblastic growth. Fibroblasts are responsible for the production of the mucopolysaccharide ground substance.

The lymphatics develop, new nerve fibers are formed, and hyalinization occurs. Scar tissue also forms. Collagen turnover increases and remodeling in the scar continues. The gross appearance of remodeling scars suggests that collagen fibers are altered and rewoven into different architectural patterns over time. Initially, the strength of the wound is only that of the clot, which cements the cut surfaces together. Later on, various changes take place in the wound healing process. At the end of wound healing, the tensile strength of the wound corresponds to the increase in the amount of collagen formed.

Hsiao et al. (2012) indicated that an increase in weight of granulation tissue was due to the presence of higher protein content. *Angelica sinensis* leaf ethanolic extract was used to treat various forms of skin trauma as confirmed by biomolecular assays involving collagen secretion, migration, and measurements of reactive oxygen species; their results were consistent with proteomic analysis. *Pyrostegia venusta* leaf ethanolic extract showed potent wound-healing capacity as evidenced by wound contraction and increased tensile strength, while HYP and hexosamine expression were also correlated with healing (Roy et al. 2012). Ethanolic and aqueous extracts of *Delonix regia* flowers had a wound-healing effect in albino rats using incision and excision wound models. Wound-healing activity was assessed by the rate of wound contraction, period of epithelialization, tensile strength and estimation of HYP content. The extracts significantly promoted healing, as evidenced by an increase in wound-breaking strength, percentage of wound contraction, increased HYP content and decreased epithelialization period when compared with the control, suggesting the possible utilization of this plant to enhance wound healing (Khan et al. 2012). Different extracts from the roots of *Plumbago indica* were evaluated for their wound-healing activity using an excision wound model (Kumar et al. 2013). The ethanolic extract possessed better wound-healing activity than the chloroform and hexane extracts, and it was more effective than the commercial wound-healing agent burnol, with complete wound healing taking place on the 9$^{th}$ PWD. The extract also showed rapid epithelization, better wound closure, and reduced infection. The hexane extract also showed good wound-healing capacity while the chloroform extract was as ineffective as the reference control.

The word healing means replacement of destroyed tissue by living tissue. Somen (2001) claimed that the four basic processes that take place in wound healing are inflammation, wound contraction, epithelialization, and granulation tissue formation. Immediately after disruption of tissue integrity, inflammation starts. Platelets become adherent and, together with clotting factors, form a hemostatic plug to stop bleeding from the small vessels. Two prostaglandins ($PGE_1$ and $PGE_2$) are released in the inflamed area and seem to be the final mediators of acute inflammation and may play a chemotactic role for white cells and fibroblasts. Actively motile white cells migrate into the wound and start engulfing and removing cellular debris and injured tissue fragments. Leukotaxin, a peptide formed in the damaged tissue by the enzymatic destruction of albumin, is thought to be the chemotactic agent, attracting leukocytes into the wounds. Monocytes must be present to create normal fibroblasts production. Due to the effect of UA and the ME of *C. gouriana*, the formation of collagen fibers most likely increased.

## REFERENCES


Abirami A, Nagarani G, Siddhuraju P. 2015. Hepatoprotective effect of leaf extracts from *Citrus hystrix* and *C. maxima* against paracetamol-induced liver injury in rats, Food Sci Human Wellness 4: 35-41

Alam J, Mujahid M, Badruddeen, Jahan Y, Bagga P, Rahman MA. 2016. Hepatoprotective potential of ethanolic extract of *Aquilaria agallocha* leaves against paracetamol-induced hepatotoxicity in SD rats, J Trad Compl Med 10: 1-5.

Amjad-Iranagh S, Golzar K, Modarress H. 2014. Molecular simulation study of PAMAM dendrimer composite membranes, J Mol Mod 2: 2119

Amin KM, Anwar MM, Kamel MM, Kassem EM, Syam YM, Elseginy SA. 2013. Synthesis, cytotoxic evaluation and molecular docking study of novel quinazoline derivatives as PARP-1 inhibitors, Acta Poloniae Pharm 70:833-849.

Anthony D, Metcalfe M, Ferguson WJ. 2007. Tissue engineering of replacement skin: the crossroads of biomaterials, wound healing, embryonic development, stem cells and regeneration, J Royal Soc Intl 4: 413-437.

Arafat AS, Arun A, Ilamathi M, Asha J, Sivashankari PR, D'Souza CJ, Sivaramakrishnan V, Dhananjaya BL. 2014. Homology modeling, molecular dynamics and atomic level interaction study of snake venom 5' nucleotidase, J Mol Model 20: 2156.

Azad S. 2002. Essentials of Surgery. Paras Medical Pub, Hyderabad:

Borhani DW, Shaw DE. 2012. The future of molecular dynamics simulations in drug discovery, J Comp Aid Mol 26: 15-26.

Chowdhury A, Paul P, Choudhury MD. 2013. High throughput screening of 7-methylpicene-1, 2-diol as arylamine *N*-acetyltransferase (NAT) inhibitor to establish an isoniazid supplement in anti-tubercular therapy, Comb Chem High Through Screen 16: 721-725.

Ehrlich HP, Hunt TK. 1969. The effect of cortisone and anabolic steroids on the tensile strength of healing wounds, Ann Surg 57: 117-119.

Ganachari MS, Kumar S, Patel A. 2005. Wound healing activity of *Saussurea lappa* roots, Indian Drug 42: 295-298.

Garg VK, Paliwal SK. 2011. Wound-healing activity of ethanolic and aqueous extracts of *Ficus benghalensis*, J Adv Pharma Technol Res 2: 110-114.

Geethalakshmi R, Sakravarthi C, Kritika T, Arul Kirubakaran M, Sarada DVL. 2013. Evaluation of antioxidant and wound healing potentials of *Sphaeranthus amaranthoides* Burm, Bio Med Res Intl 9: 1-7.

Ghosh MN. Fundamentals of Experimental Pharmacology, Kolkata, India: Scientific Book Age 1984

Guo S. Moore TC, Iacovella CR, Strickland LA, McCabe C. 2013. Simulation study of the structure and phase behavior of ceramide bilayers and the role of lipid head group chemistry, J Chem Theory Comp 12: 5116-5126.

Harsha VH, Hebbar SS, Shripathi V, Hegde G.R. 2003. Ethnomedicobotany of Uttara Kannada district in Karnataka, India - plants in treatment of skin diseases, J Ethnopharma 84: 37-40.

Hsiao CY, Hung CY, Tsai TH, Chak KF. 2012. A study of the wound healing mechanism of traditional Chinese medicine, *Angelica sinensis*, using a proteomic approach, Evidence-Based Compl Alternative Med 1:1-14.

Jain N, Jain R, Jain A, Jain DK, Chandel HS. 2010. Evaluation of wound-healing activity of *Acorus calamus* Linn, Nat Prod Res 24: 534-541

Kanai L, Mukherjee. 2000. Medical Laboratory Technology, New Delhi: Tata McGraw Hill Ltd.

Kepp KP, Dasmeh P. 2014. A model of proteostatic energy cost and its use in analysis of proteome trends and sequence evolution, PLoS ONE 28: 9.

Khan MA, Saxena A, Tabassum F, Gaurav S, Goud V, Asif H. 2012. Study of wound healing activity of *Delonix regia* flowers in experimental animal models, Amer J Pharm Techno Res 2: 380-390.

Kumara Swamy HM, Krishna V, Shankarmurthy K, Abdul Rahiman B, Mankani KL, Mahadevan KM, Harish BG, Raja Naika H. 2007.

Wound healing activity of embelin isolated from the ethanol extract of leaves of *Embelia ribes* Burm, J Ethnopharmacol 109: 529-534.

Kumar SJ, Balavigneswaran T, Prakash CK, Natheer Hassan S, Srinivasakumar KP. 2013. Excision wound healing and antioxidant activity of different root extract of *Plumbago indica*, Med Plants Res 3:13-19.

Manjunatha BK, Krishna V, Vidya SM, Mankani KL, Manohara YN. 2007. Wound healing activity of *Lycopodium serratum*, Indian J Pharma Sci 69: 283-287

Manjunatha BK, Krishna V, Pullaiah T. 2001. Flora of Davanagere district, Karnataka, India, New Delhi: Regency Pub

Mahanta S, Pilla S, Paul S. 2013. Design of novel geldanamycin analogue hsp90 alpha-inhibitor *in silico* for breast cancer therapy, Medical Hypo 81: 463-469.

Manjunatha BK, Vidya SM, Rashmi KV, Mankani KL, Shilpa HJ, Singh SDJ. 2005. Evaluation of wound healing potency of *Vernonia arborea* Hk, Indian J Pharma 37: 223-226.

Meenakshi S, Raghavan G, Virendra N, Ajay KSR, Shanta M. 2006. Antimicrobial, wound healing and antioxidant activity of *Plagiochasma appendiculatum* Lehm. et Lind, J Ethnopharmacol 107: 67-72.

Minakshi C, Sushma M. 2006. Evaluation of phytoconstituents of *Terminalia arjuna* for wound healing activity in rats, Phytother Res 20:799-805

Morton JJP, Malone MH. 1972. Evaluation of vulnerary activity by an open wound procedure in rats, Arch Inter Pharmacodynamics Theory 1: 117-126.

Nayak BS, Pinto Pereira LM. 2006. *Catharanthus roseus* flower extract has wound-healing activity in Sprague Dawley rats, BMC Compl Alter Med 6 (41): 1-6.

Newman DJ, Cragg GM, Snader KM. 2003. Natural products as sources of new drugs over the period 1981-2002. J Nat Prod 66: 1022-1037.

Patronov A, Dimitrov I, Flower DR, Doytchinova I. 2011. Peptide binding prediction for the human class II MHC allele HLA-DP2: a molecular docking approach. BMC Struct Biol 14: 11-32.

Patil MB, Jalalpure SS, Nagoor VS. 2004. Wound healing activity of the roots of *Eclipta alba* Linn, Indian Drugs 41: 40-45.

Pather N, Viljoen AM, Kramer BA. 2011. Biochemical comparison of the *in vivo* effects of *Bulbine frutescens* and *Bulbine natalensis* on cutaneous wound healing, J Ethnopharm 133: 364-370

Preethi KC, Kuttan R. 2009. Wound healing activity of flower extract of *Calendula officinalis*, J Basic Clin Physiol Pharmacol 20: 73-79.

Pizzo F, Lombardo A, Manganaro A, Benfenati E. 2013. *In silico* models for predicting ready biodegradability under REACH: a comparative study. Sci Total Env 2013. 463-464: 161-168.

Reinke JM, Sorg H. 2012. Wound repair and regeneration, Eur Surg Res 49: 35-43.

Romero-Cerecero O, Zamilpa A, González-Cortazar M, Alonso-Cortés D, Jiménez-Ferrer E, Nicasio-Torres P, Aguilar-Santamaría L, Tortoriello J. 2013. Pharmacological and chemical study to identify wound-healing active compounds in *Ageratina pichinchensis*, Planta Med 79:622-627.

Roy P, Amdekar S, Kumar A, Singh R, Sharma P, Singh V. 2012. *In vivo* antioxidative property, antimicrobial and wound healing activity of flower extracts of *Pyrostegia venusta* (Ker Gawl) Miers. J Ethnopharmacol 140:186-192

Rubin E, Hutterer F, Popper H. 1963. Cell proliferation and fiber formation in chronic $CCl_4$ intoxication-A morphogenic and chemical study, Amer J Pathol 45: 715-728.

Singh SD, Krishna V, Mankani KL, Manjunatha BK, Vidya SM, Manohara, Solanki R, Shiv Kumar P, Vipin M, Manoj M. 2012. Evaluation of wound healing activity of ethanolic extract of *Ocimum basilicum* leaves in male albino rats, Intl J Drug Res Technol 2: 208-211.

Somen D. 2001: A Concise Textbook of Surgery (3rd ed.), Old Mayor's Court: Calcutta, India.

Trease GE, Evans WC. 1983. Pharmacognosy (12th ed.), Bailliere Tindall Pub., Eastbourne.

Vijaykumar PR, Arulmozhi S, Purnima A, Sridhar Y. 2008. Wound healing and antioxidant activities of *Morinda citrifolia* leaf extract in rats, Iranian J Pharma and Ther 7: 49-52.

Weiss A, Attisano L. 2013. The TGF beta superfamily signaling pathway, Dev Biol 2: 47-63

Woessner JF. 1963. The determination of hydroxyproline in tissue and protein samples containing small proportions of the imino acid, Archives of Biochem 93: 440-447.

Zhang DL, Gu LJ, Liu L, Wang CY, Sun BS, Li Z, Sun CK. 2008. Effect of Wnt signaling pathway on wound healing, Biochem Biophys Res Comm 378: 149-151.

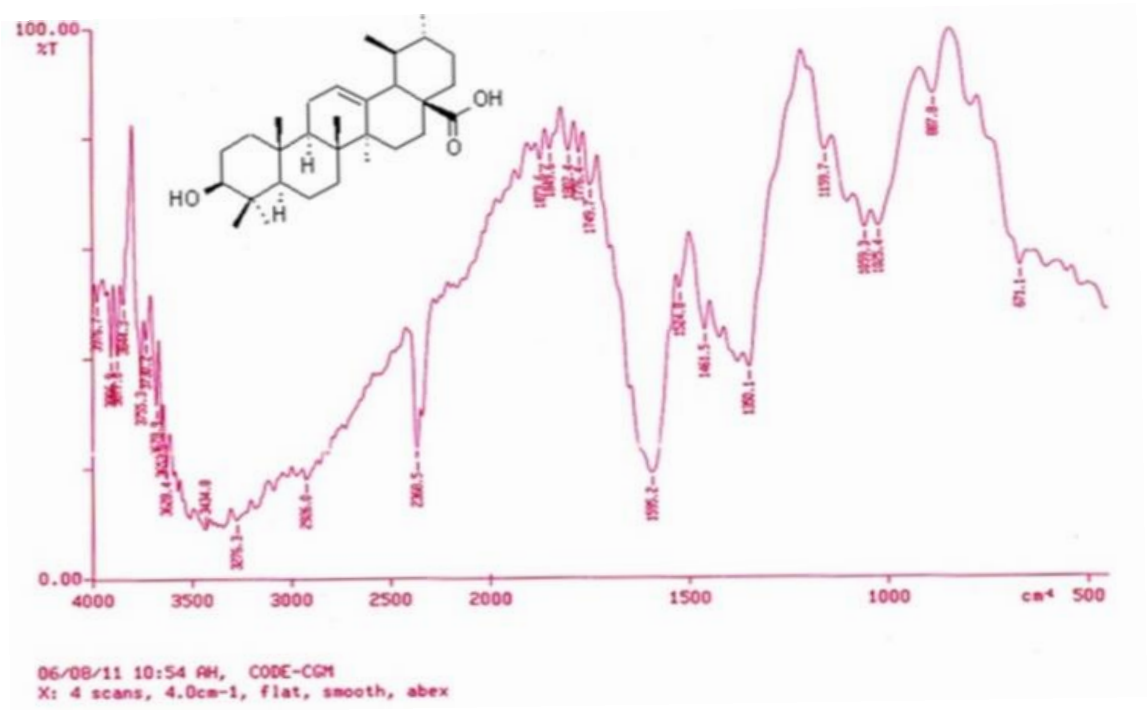


**Figure 1S.** IR spectrum of ursolic acid showing absorptions bands at 3434.8 $cm^{-1}$ for the hydroxyl group and 2926.0 and 2368.5 $cm^{-1}$ for the terminal methylene groups

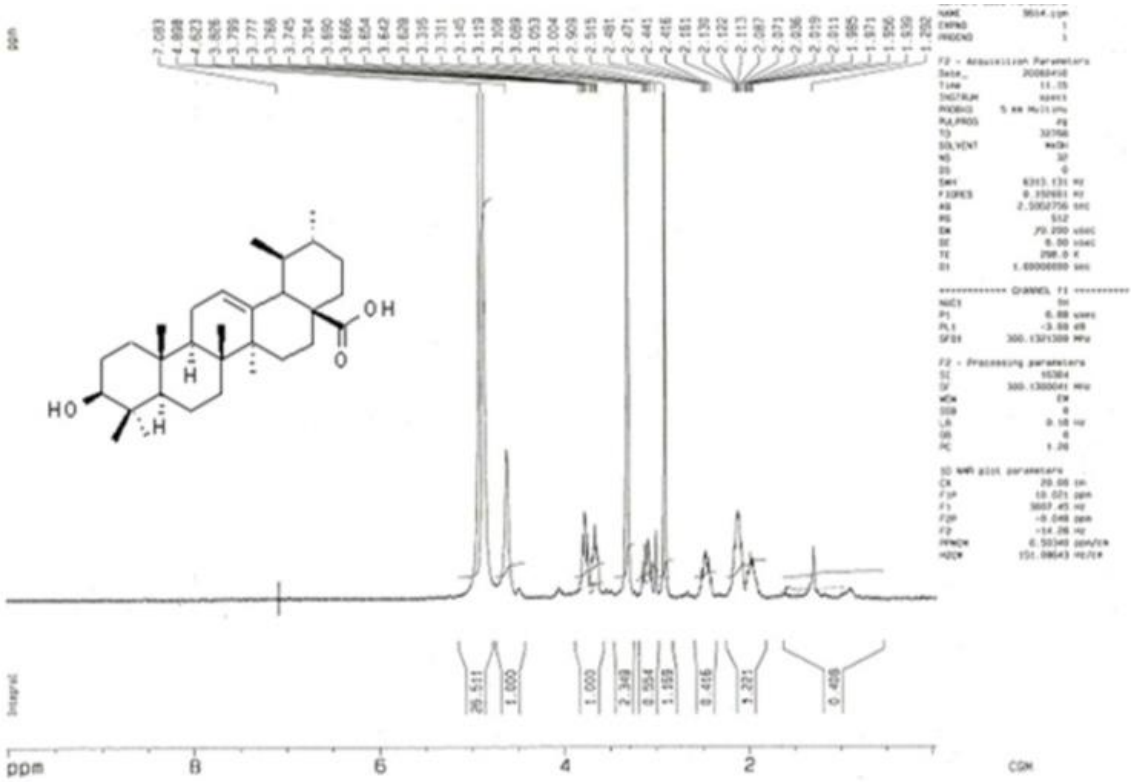


**Figure 2S.** [1]H NMR spectrum of ursolic acid revealed the presence of terminal methyl groups at δ 0.88 to δ 0.9 and a multiplet at δ 4.52 due to olefinic protons.

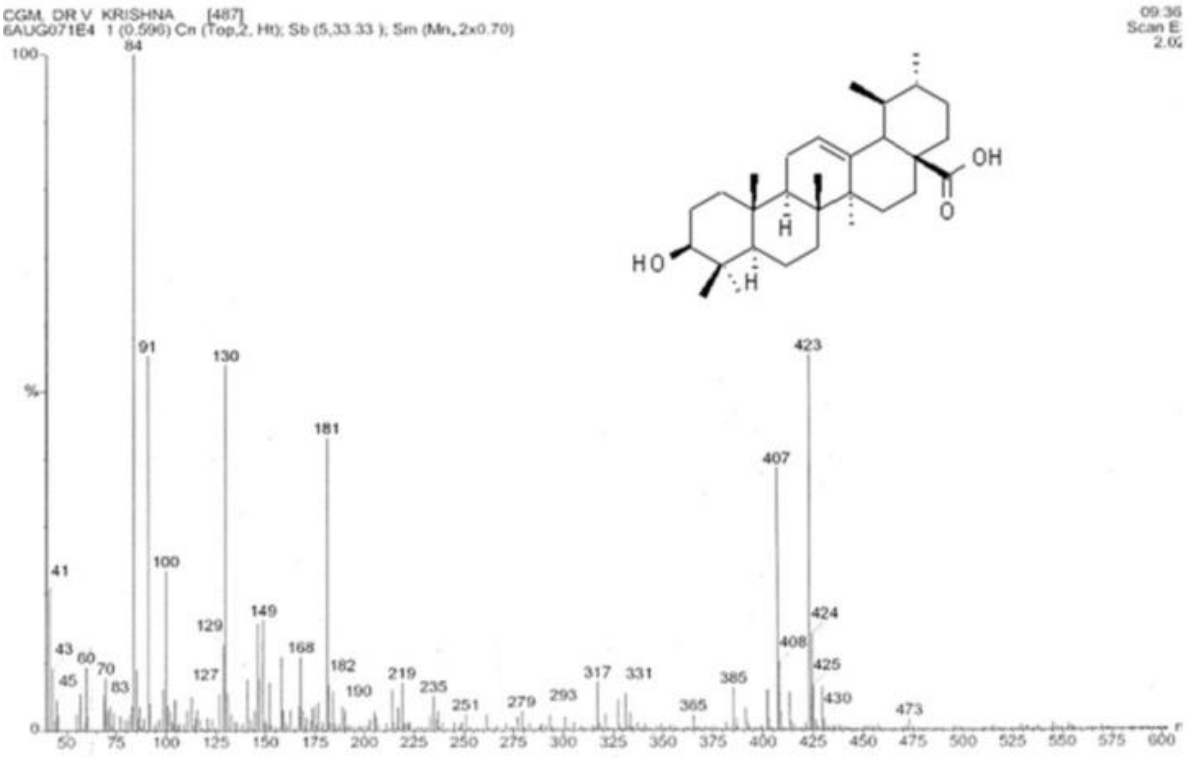


**Figure 3S.** $ES^+$ mass spectrum of ursolic acid showing a molecular ion peak at m/z 475 corresponding to the molecular formula $C_{30}H_{48}O$